Supporting Information Online for

Isolation of >1 nm Diameter Single-Wall Carbon Nanotubes Species Using Aqueous Two Phase Extraction

Jeffrey A. Fagan,[1,*] Erik H. Hároz,[2] Rachelle Ihly,[3] Hui Gui,[4] Jeffrey L. Blackburn,[3] Jeffrey R. Simpson,[5] Stephanie Lam,[1] Angela R. Hight Walker,[5] Stephen K. Doorn[2] and Ming Zheng[1]

1: Materials Science and Engineering Division, National Institute of Standards and Technology, Gaithersburg, MD 20899

2: Center for Integrated Nanotechnologies, Los Alamos National Laboratory, Los Alamos, New Mexico 87545

3: National Renewable Energy Laboratory, Golden, CO 80401

4: Department of Chemical Engineering and Materials Science, University of Southern California, Los Angeles, CA 90089

5: Semiconductor and Dimensional Metrology Division, National Institute of Standards and Technology, Gaithersburg, MD 20899

*Corresponding Author: jfagan@nist.gov

Certain equipment, instruments or materials are identified in this paper in order to adequately specify the experimental details. Such identification does not imply recommendation by the National Institute of Standards and Technology (NIST) nor does it imply the materials are necessarily the best available for the purpose.

Single-Wall Carbon Nanotube Sources and Acronyms

- High pressure CO disproportionation (HiPco)
- Plasma torch (PT)
- Laser-vaporization (LV)
- Electric arc (EA)
- Floating catalyst decomposition (FCCD) [1,2]

Preparation of parent nanotube dispersions for separation

Dispersion of the raw single-wall carbon nanotube (SWCNT) soot into a liquid phase as individual particles is necessary for the reported processing steps. For dispersion, each SWCNT powder was mixed with sodium

deoxycholate (DOC) solution in water at concentrations of 1 mg/mL and 20 g/L, respectively. These mixtures were exposed to tip sonication (30 min or 1 h, 0.9 W/mL) to generate a dispersion of the nanotubes in the surfactant solution, and then subsequently centrifuged (Beckman J-2 centrifuge, JA-20 rotor, 1884 rad/s, 2 h) to remove gross impurities (collecting the supernatant). Aliquots (≅ 8.2 mL) of the supernatant were then layered on top of ≅ 28 mL of either 10 % (HiPco), 12 % (LV and EA SWCNTs) or 15 % (FCCD) (volume/volume) iodixanol and 10 g/L DOC solution. These centrifuge tubes were then ultracentrifuged for ≈ 3 h in a VTi-50 rotor (Beckman-Coulter) at 5240 rad/s (50k RPM) at 20 °C. Photographs of the separated SWCNTs within the centrifuge tubes denoting the separated layers are shown in Figure S1. The bands in the middle of the tubes shown in Figure S1 contain well-individualized and primarily rigid SWCNTs; the upper band (when present), outlined with orange dashes, has previously been shown to contain the empty (closed ended) SWCNTs, and the lower band, outlined with red dashes, the water-filled SWCNTs. Not all SWCNT populations contain end-capped SWCNTs, and thus do not display a band corresponding to empty SWCNTs; this is the case for the far right population in Figure S1. All collected SWCNT populations were concentrated and adjusted towards a DOC concentration of 10 g/L using iterative concentration dilution cycles in a pressurized ultrafiltration stirred cell (Millipore) with either a 100 kD MW or 300 kD MW cutoff membrane. These dispersions were then used as the top level parent, *i.e.* before M/S sorting, in the main paper.

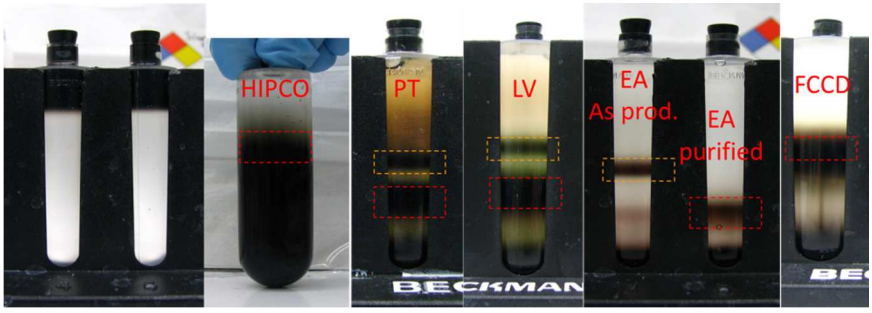

Figure S1. Photographs of the rate based separation of empty and water-filled SWCNTs from denser aggregates and faster (slower) moving impurities before (left hand tubes) and after the separation. In the deterministic velocity limit, each component in the initial layer translates downward (relative to the geometry as photographed) through the liquid column at a rate proportional to their buoyant mass (density difference x volume), and inversely proportional to their hydrodynamic size. Thus water-filled nanotubes translate further than empty (closed ended) nanotubes, and morphologically defective (i.e. non-straight) nanotubes and bundles travel further still, enabling separation. The location of extracted bands of empty and water-filled SWCNTs are shown by the orange and red dashed boxes, respectively.

HiPco Synthesized SWCNT Dispersion Separation via ATPE

A commonly researched synthetic method for SWCNTs, the HiPco process and similar variants produce nanotubes with an average diameter of ≈ 1 nm. At the small diameter end of the distribution, the species present in the HiPco source material overlap with those of the CoMoCat material for which we previously reported a great degree of diameter resolution,[3] and so are not the focus of this contribution. Photographs and

spectral data from the separation of larger semiconductors, and of metallic SWCNTs, from the parent dispersion shown in Figure 1 of the main text are shown in Figures S2 and S3. In both figures, the absorbance spectra of the metallic/semiconducting separated parent dispersion is shown as the top trace, with the following traces reported in the order of least to greatest sodium dodecyl sulfate (SDS) concentration required to extract the SWCNTs to the top phase going from the top to the bottom. For both figures, the locations of the absorbance features (and identities of the SWCNT species generating the transitions) generally follow the trend of the largest SWCNTs being extracted to the top phase at lower SDS concentrations than smaller diameter nanotubes. Figure S4, which summarizes the apparent diameter versus fraction number trend makes this clear. However, as discussed in the main contribution, there is a cluster of SWCNT species of approximately 1.05 nm in diameter (carbon center – carbon center definition) that behave in a manner inconsistent with this trend. In particular this includes the (8,8) armchair metallic species, and several semiconducting species including the (8,7) and (10,5). A clear visual proof of the unusual (8,8) separation is shown in the right hand side (RHS) of Figure S2, in which the pink, (8,8) – rich, resides in the bottom dextran phase, with a yellow extracted poly-ethylene glycol (PEG) phase containing the smaller diameter (6,6) and (7,7) metallic species on top.

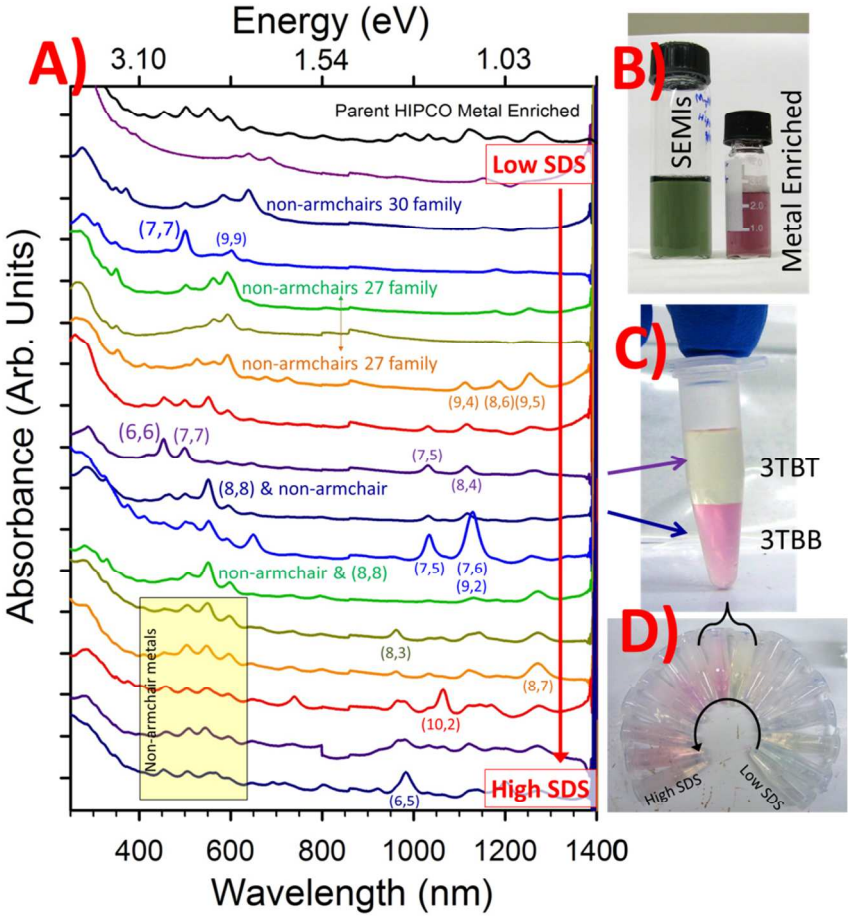

Figure S2. A) Absorbance spectra of diameter separated HiPco metallic SWCNT fractions. Clear separation of different species in each fraction is observed in the changing distribution and locations of peaks in the

absorbance plot, particularly in the region from 450 nm to ≈ 650 nm in which metallic SWCNTs have their M11 optical transitions. Clearly identifiable species are noted with matching color text adjacent to the identified peak; several semiconducting contaminant species are also identified to facilitate comparisons in extraction order. The data are scaled for presentation such that the highest intensity feature in the 450 nm to 800 nm region is equal to 1.25, showing only the range from 0.25 to 1.25 for each trace to enable better comparison of the peak locations, which are more important than the absolute intensities relative to underlying baseline absorbance in this case; progressive scans are offset by a value of 1 (all intensity values are scaled and thus unitless). B) Photograph showing the color of the parent metallic and semiconducting enriched HiPco dispersions prior to diameter separation. C) Photograph showing the split of fraction 3TBT from 3TBB (arrows indicate the two absorbance spectra corresponding to the two phases) demonstrating that the (6,6) and (7,7) both are extracted into the top phase at a lower SDS concentration than the (8,8) SWCNT in violation of the typical larger diameter first order. This is discussed in the main contribution. D) Photograph of all the extracted fractions from the diameter separation, in order, corresponding to the spectra in the absorbance plot.

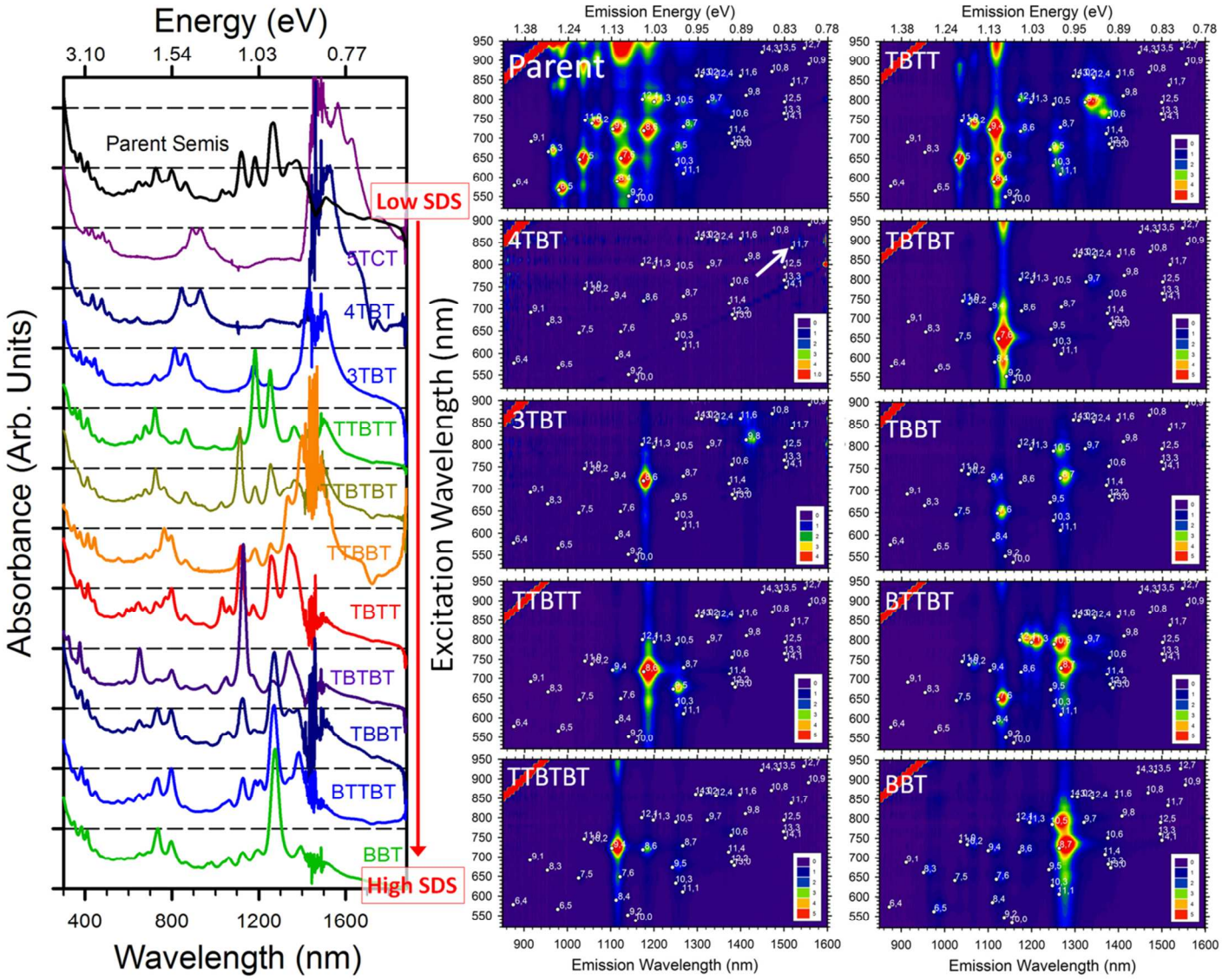

Figure S3. Absorbance and photoluminescence spectra of diameter separated HiPco semiconducting SWCNT fractions. Although the separation is rough, clear separation of different species in each fraction is observed both in the absorbance plot and more explicitly in the fluorescence data. The noise at ≈ 1450 nm in the absorbance figure is due to the inexact subtraction of the strong water absorbance from the absorbance of dilute

SWCNT fractions at that wavelength. For PL, the samples were diluted into DOC in D_2O to enable observation of species emitting between 850 nm and 1600 nm, however the emission of the 5TC and 4TBT fractions primarily occurs at wavelengths beyond the range of this instrument's detector (≈ 1600 nm). Lastly, of note, the PL data for the BTTBT and BBT fractions show that the (10,5) and (8,7) species are extracted into the PEG phase at unusually large SDS concentrations, beyond that required to extract significantly smaller diameter SWCNTs; this phenomenon is addressed in the main text.

Plot of HiPco Semiconducting SWCNT Diameter versus the Extracted Fraction Number

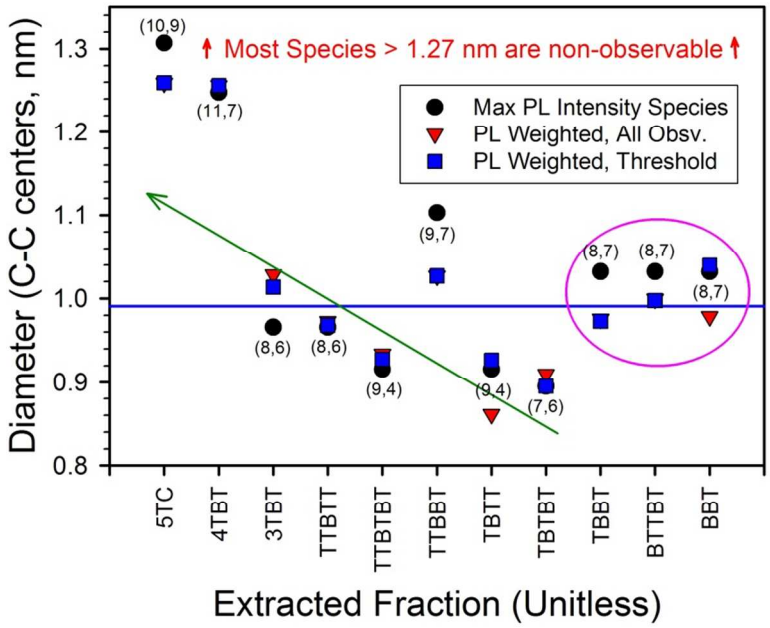

Figure S4. Several metrics of the average SWCNT diameter distribution observed in the ATPE fractions for the HiPco semiconducting SWCNTs shown in Figure S3. These metrics are the diameter of the brightest observed SWCNT, the emission intensity weighted average of the observed species (not correcting for intrinsic efficiency effects), and an emission intensity weighted average including only species above 20 % of the maximum intensity species. Instrument limitations make most SWCNTs larger than ≈ 1.27 nm in diameter non-observable, and thus potentially limit the apparent average diameter for the lowest SDS extracted fractions (5TCT end). Despite this limitation, the clear trend of diameter separation as a function of SDS concentration (green eyeguide line) is observed despite the inexactness of the metrics. The fractions in the ellipse contain most of the species of ≈ 1 nm in diameter that, as discussed in the main paper, separate unusually compared to most other (*n,m*) species.

Separation Results for LV and EA Metallic SWCNTs

Separation of the metallic species in the LV source SWCNT population overlaps significantly with the data shown in Figure 2D of the main contribution, and thus were not reported in the primary manuscript for space considerations. The results of iterative diameter separation via the same methodology as in the primary contribution for the metallic species (from a somewhat armchair enriched fraction) is reported in Figure S5. As in the other data sets, clear resolution of specific SWCNT species is readily achievable by iterative manual

extraction in the general trend order of largest diameters at lesser SDS concentrations to smallest diameters at greater SDS concentrations.

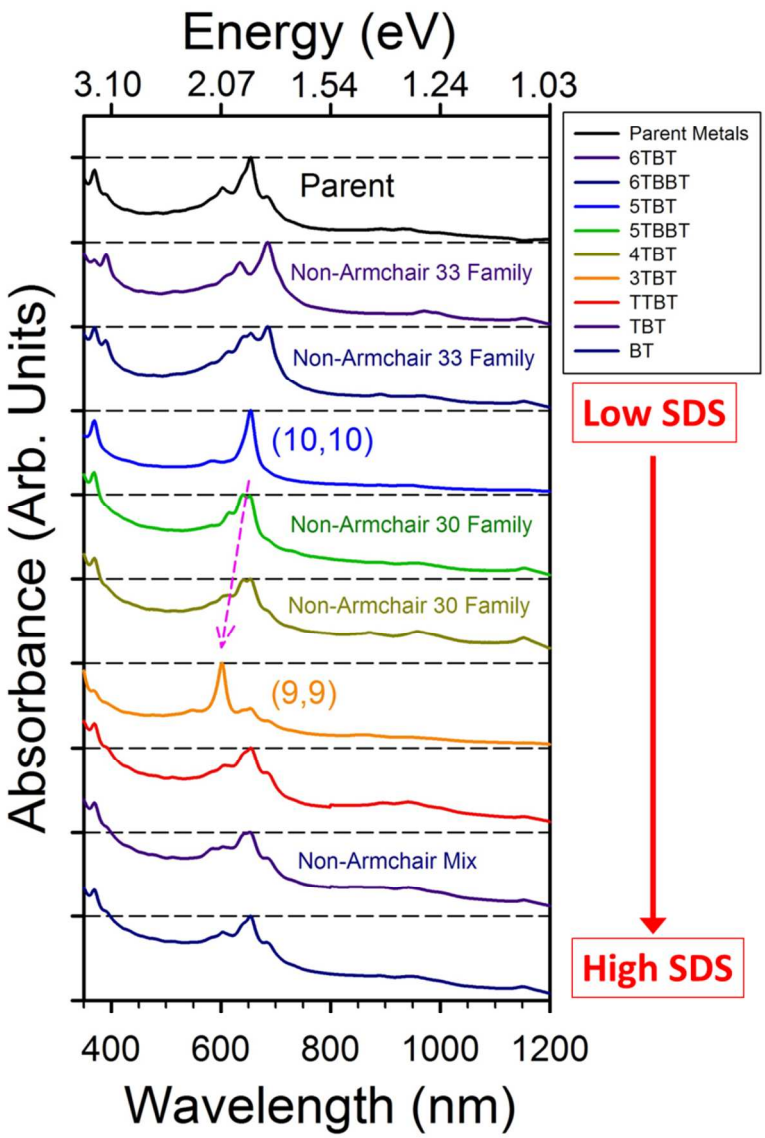

Figure S5. Absorbance spectra of metallic SWCNT fractions from LV metallic enriched parent dispersion in order from the least (penultimate top) to greatest SDS concentration required for extraction of the SWCNTs to the top phase. The clear trend of larger to smaller average SWCNT diameter for each fraction with respect to this order is visible in the shift of the optical transitions from longer to shorter wavelengths, particularly in the top 6 extracted fractions; the bottom three fractions likely contained a combination of aggregates and several non-armchair species. The armchair species is the largest in diameter for each $2n + m$ family.

Separation of the metallic species from the EA source SWCNT population was performed on a very dilute sample, and thus was not separated into as many fractions as reported for the samples in the primary manuscript. Even so, the results of iterative diameter separation via the same methodology as in the primary contribution for the metallic species (from a somewhat armchair enriched fraction) are reported in Figure S6. Even with the dilute sample severely hindering manual extraction because colors were faint, the results demonstrate that clear resolution of specific SWCNT species is readily achievable by iterative manual

extraction, and in the same general trend order of largest diameters at lesser SDS concentrations to smallest diameters at greater SDS concentrations. An interesting observation is that comparison with Figure S5 indicates that the non-armchair 33 or 36 family SWCNTs may not be uniform in whether they partition at lesser or greater SDS concentrations than the (10,10) armchair SWCNT. The 33 family ranges in average diameter from approximately (1.49 to 1.29) nm, and the 36 family from (1.63 to 1.41) nm using the formula $d = 0.0783\sqrt{n^2 + m^2 + nm}$ from [4]. The (10,10) SWCNT is 1.36 nm in diameter by this formula, in the middle of the 33 family diameter range, and thus perhaps a combination of the diameter effect, and the tendency that non-armchair species are extracted at greater SDS concentrations for otherwise uniform conditions are responsible for this observation; the distribution of non-armchair species present may also be vastly different, as insufficient data is available to distinguish them via their absorbance spectra.

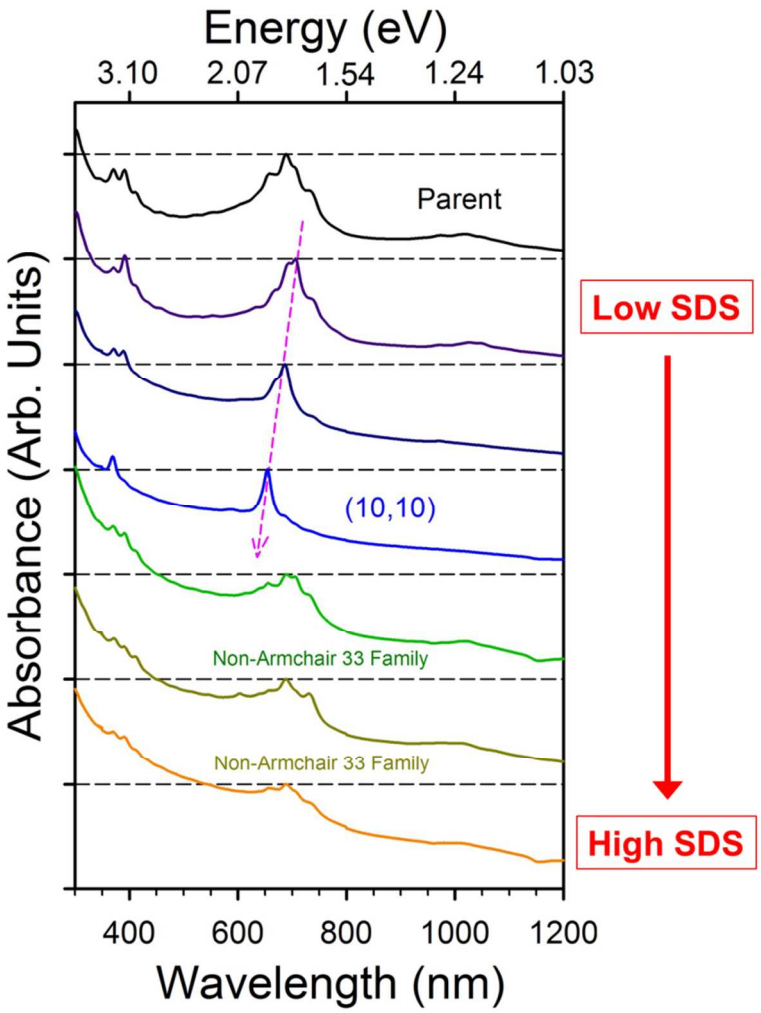

Figure S6. Absorbance spectra of metallic SWCNT fractions from the empty metallic (armchair enriched) EA parent dispersion in order from the least (penultimate top) to greatest SDS concentration required for extraction of the SWCNTs to the top phase. The clear trend of larger to smaller average SWCNT diameter for each fraction with respect to this order is visible in the shift of the optical transitions from longer to shorter wavelengths, particularly in the top 3 extracted fractions; the bottom three fractions appear to contain a

combination of several non-armchair species, most likely from the 33 and 36 families. The armchair species is the largest in diameter for each $2n + m$ family.

Additional Separation Results for Water-Filled PT and EA SWCNTs

Since most results in the main contribution and SI are shown for the separation of empty (non-accessible interior) nanotubes, we demonstrate below that the same phenomenon occurs for, and can be applied to, the more populous water-filled nanotubes that are found in dispersion after chemical treatment of the parent soot or simply from dispersion processing. Example data for separations of water-filled PT and EA SWCNTs are shown in Figures S7 and S8. Because the samples were not separated by metallic and semiconducting nature prior to separation, the color changes in the photographs are dominated by the changing distribution of both SWCNT types (the combination of whose absorbance spectra affect the visual perception of the color in sometimes non-trivial manners). The same clear diameter trend, as highlighted especially by the purple dashed arrows in Figure S7, is, however, still observed.

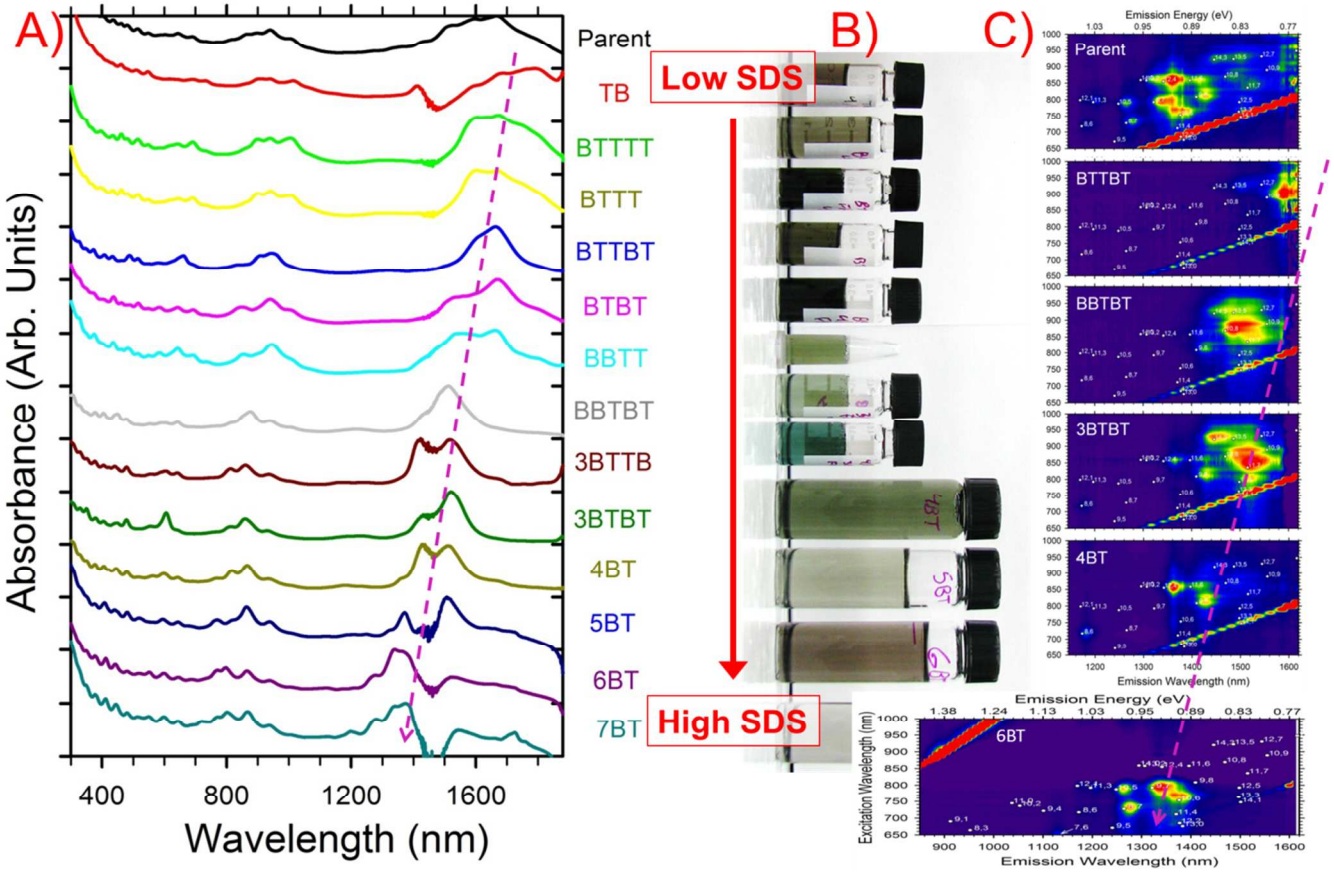

Figure S7. A) Absorbance spectra, B) photographic data, and C) fluorescence spectra from a sequential ATPE extraction experiment on water-filled PT SWCNTs; this SWCNT population was not separated by M/S functionality prior to diameter separation. As denoted by the dashed arrows in both the absorbance and fluorescence data, the average diameter of the SWCNTs extracted, as reflected in the wavelength of the absorbance and fluorescence peak locations, trends strongly with the fraction number. The SDS concentration at which the SWCNTs were extracted into the top phase was lowest for the TB and BTTTT fractions, and a

greater amount was required for each successive fraction. Instrument limitations prevented the collection of emission spectra in the fluorescence plots at wavelengths greater than 1600 nm.

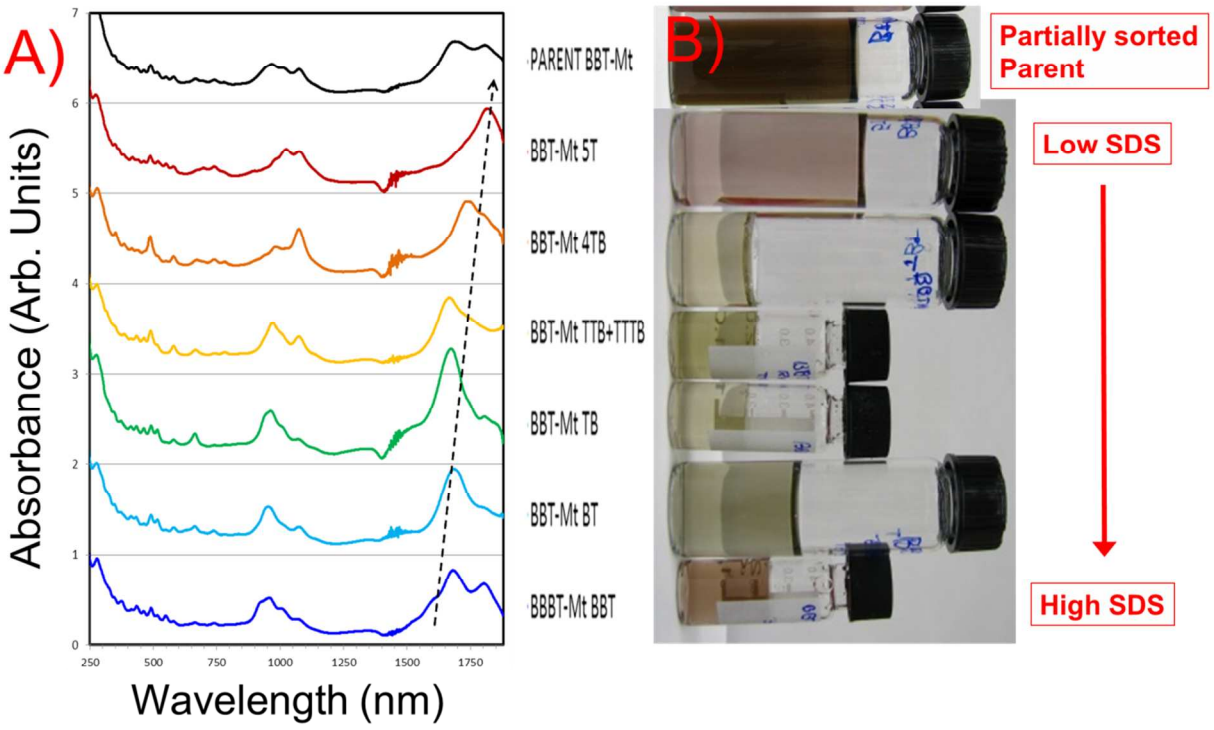

Figure S8. Data from an initial experiment on fractionating large-diameter SWCNTs with ATPE. A) Absorbance spectra, and B) photographic data from a sequential ATPE extraction experiment on water-filled EA SWCNTs; this SWCNT population was only poorly separated by M/S functionality prior to diameter separation, and the M/S sort was attempted after a poor partial separation by diameter in a previous diameter separation attempt. As denoted by the dashed arrow in the absorbance data, the average diameter of the SWCNTs, as reflected in the wavelength of the absorbance peak locations, trends strongly with the fraction number. The SDS concentration at which the SWCNTs were extracted into the top phase was lowest for the top fraction, and a greater amount was required for each successively lower fraction. Subsequent experiments (in primary manuscript) were conducted with empty EA SWCNTs and after clean metal-semiconducting separation to enable better resolution.

Additional Raman Scattering Results on Empty EA SWCNT Separation in Figure 7

Additional resonant Raman spectra results at 458 nm excitation for the same set of samples reported in Figure 7 of the main contribution. All colors map in the same manner. The resonant radial breathing mode peak features clearly change from fraction to fraction, indicating a high degree of separation between similar diameter species.

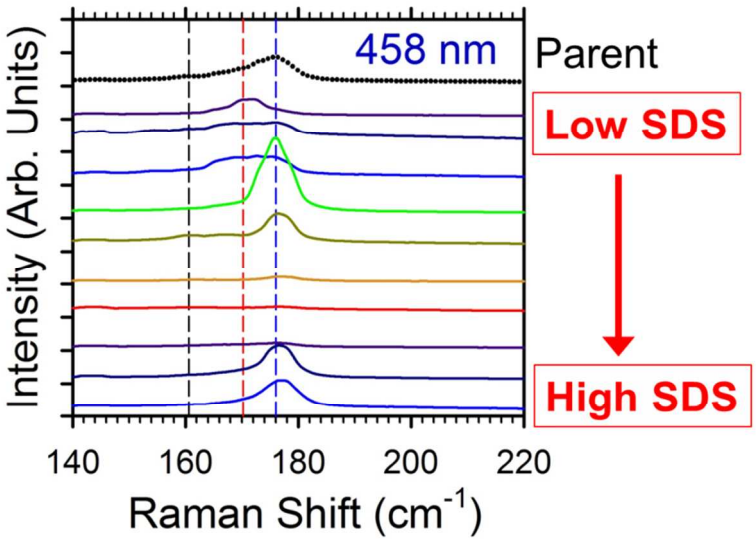

Figure S9. Resonance Raman spectra for the parent empty semiconducting-enriched EA SWCNTs shown in Figure 7 of the main contribution and its daughter fractions after diameter sorting. Colors correspond to the same fractions as in the text. The parent sample's spectra is shown in dots rather than a line plot to show the instrumental resolution, which changes as a function of the excitation wavelength. All spectra are scaled by the same factor; as the samples were approximately the same concentration (estimate based on similar absolute absorbances), the appearance/absence of RBM features is indicative of the presence/absence of specific (*n,m*) SWCNTs in each sample. RBM/E_{33} and RBM/E_{44} pair values are not sufficiently well described in the literature to assign the (*n,m*) species visible in the Figure.

Close Up of Absorbance Spectra for Samples in Figure 8

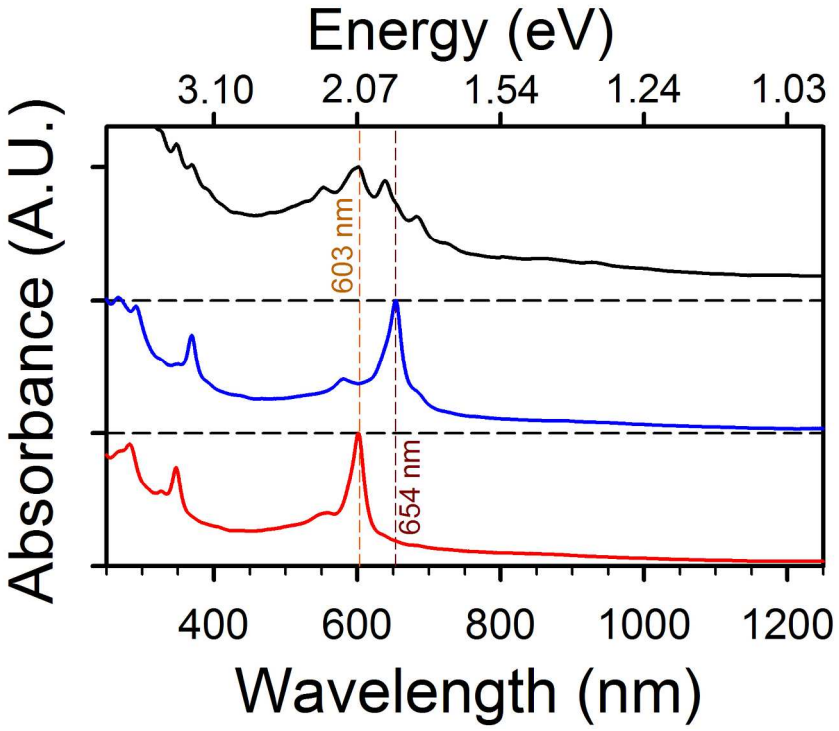

Figure S10. Absorbance spectra of the parent metallic enriched PT dispersion (top) and daughter (10,10) (middle) and (9,9) (bottom) rich fractions measured with Resonance Raman spectroscopy in Figure 8 of the main contribution. Vertical dashed lines show the excitation wavelengths used for the Raman excitation.

Raman RBM Region Contours for Samples in Figure 8

Separation Results on FCCD SWCNTs

FCCD SWCNTs were separated at a greater DOC concentration (0.1%) than the other SWCNT source dispersions, since FCCD SWCNTs did not partition into the bottom phase at any SDS concentration for a DOC concentration of ≈ 0.04 %. The additional DOC content, which may not be optimal, allowed for controllable partitioning of the SWCNT dispersion between the two ATPE phases at SDS concentrations of ≈ 0.15 % to 0.71 %. Clear diameter trend separation is observed, particularly for the metallic SWCNT sample (optical transition wavelengths are more linearly correlated with diameter for M_{11} transitions than for semiconducting SWCNT optical transitions). Families, and average diameters, are assigned on the basis of the optical transition wavelengths.[8] Results of separating metallic and semiconducting FCCD SWCNT dispersions are shown in Figure S11 and S12 respectively. It should be noted that the optical transitions of water-filled SWCNTs are red-shifted and significantly broader than for empty SWCNTs of the same (*n,m*).[5,6]

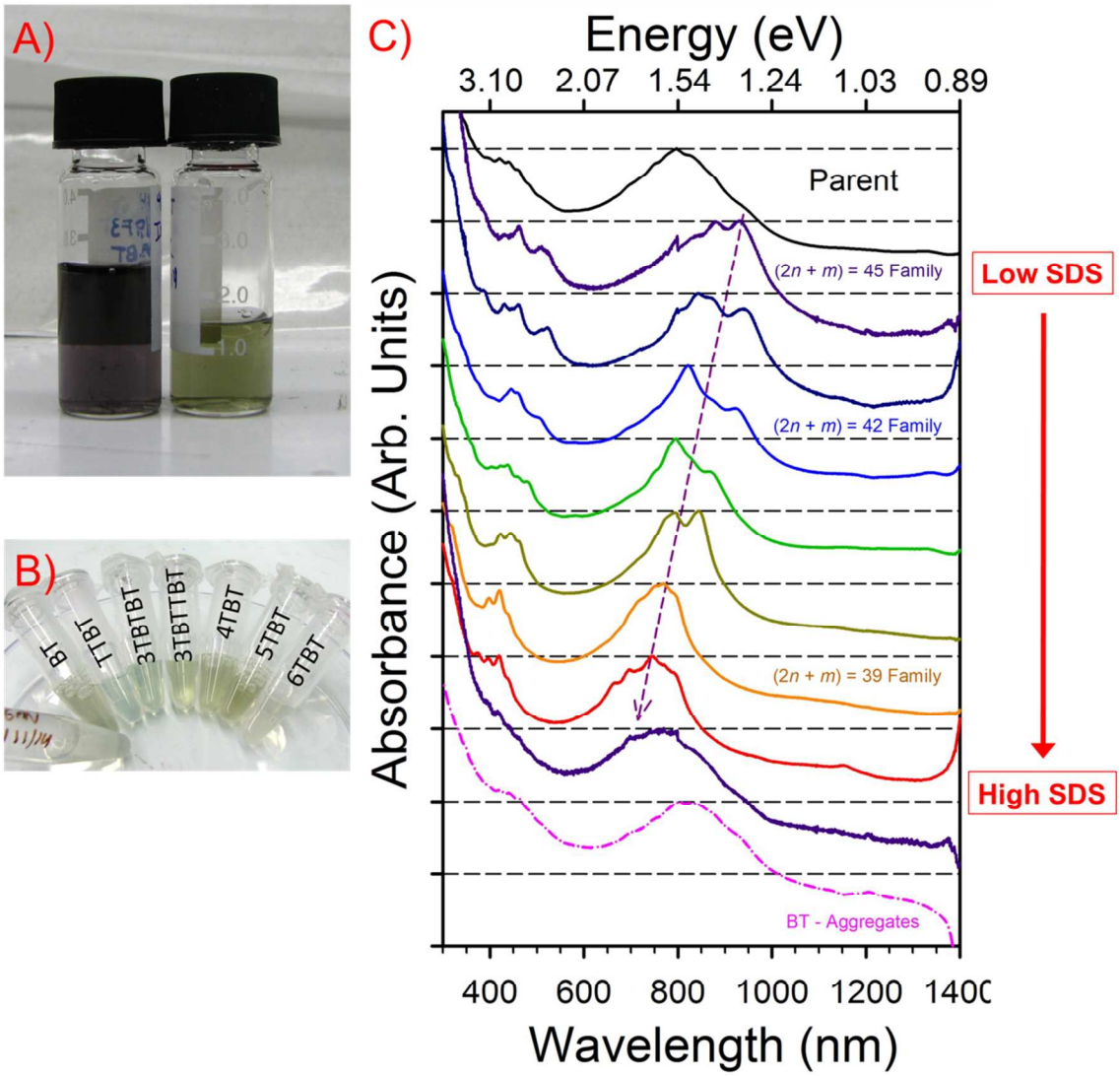

Figure S11. A) Photograph of ATPE separated large diameter FCCD SWCNTs, the purple and green vials are semiconducting and metallic enriched dispersions respectively. B) Photograph of ATPE fractions from the metallic parent dispersion. The color of the fractions ranges from peach (6TBT) to sky blue (TTBT). Fractions for the two purple spectra in panel C (7TBT and TBT) were colorless to the eye due to diluteness and so were not included in the photograph. C) Absorbance spectra of the parent metallic enriched dispersion and the daughter ATPE separated dispersions from low SDS concentration for extraction (top) to greater SDS concentration for extraction (bottom). The nominal DOC content was 1 g/L for this separation. The average diameter of the three observed metallic families, not accounting for abundance, range from 1.87 nm (45 family) to 1.74 nm (42 family) to 1.62 nm (39 family). The approximate SDS concentrations for extraction of the SWCNTs to the top phase ranged from 0.71 % (TBT lowest purple curve), to 0.5 %, 0.36 %, 0.25 % (both yellow and green curves), 0.19 % and 0.15 % (6TBT, navy blue curve); the largest average diameter fraction was pushed to the bottom phase by addition of more DOC. The dashed purple eye-guide arrow, highlighting the trend in the shift of the optical peak locations, spans 300 nm on the x-axis.

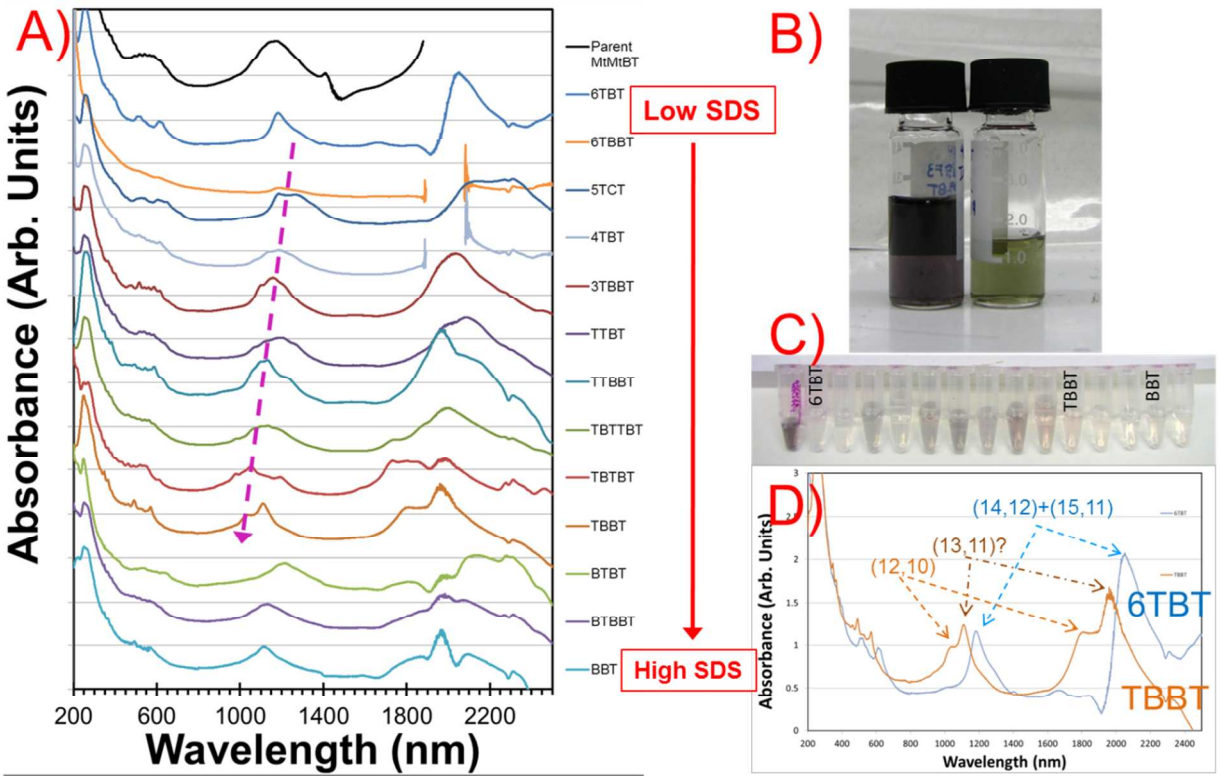

Figure S12. A) Spectra of semiconducting sorted parent FCCD dispersion and ATPE diameter sorted daughter fractions after exchange into 1 % DOC/D_2O. Significant variation in, and resolution of, the location of optical transitions is observed, especially ignoring the bottom three spectra that were likely aggregated SWCNTs. B) Photograph of purple and green vials that are semiconducting and metallic enriched parent dispersions respectively. C) Photograph of ATPE daughter fractions from the semiconducting parent dispersion after exchange into D_2O. D) Absorbance spectra of two daughter ATPE separated dispersions from low SDS concentration for extraction (6TBT) and greater SDS concentration for extraction (TBBT) showing a high degree of (*n,m*) resolution. The nominal DOC content was 1 g/L for this separation. Best estimate species identifications, using the table of [3], are shown on the figure. The diameters of these species are: (12,10) $\rightarrow$1.515 nm; (13,11) $\rightarrow$ 1.652 nm; (14,12) $\rightarrow$1.789 nm; (15,11) $\rightarrow$1.795 nm. These species all fluoresce at wavelengths longer than our detection capability. However the significant difference in apparent average diameter indicates that diameter separation is still achievable for large diameter SWCNTs.

Experimental Methods for SI Figures

Absorbance Spectra: UV-vis-NIR absorbance spectra were collected on a Cary 5000 UV-vis-NIR spectrometer from (1880 to 185) nm in 1 nm increments through a (1, 2 or 10) mm quartz cuvette with an integration time of 0.1 s/nm (2 nm slit width). The spectra of the corresponding blank surfactant solution was collected separately and linearly subtracted during data analysis.

Fluorescence Spectra: NIR fluorescence was measured on a Horiba Jobin-Yvon Nanolog-3 spectrofluorometer with a liquid nitrogen cooled InGaAs array detector and a 450 W xenon lamp. Excitation was selected using a dual grating monochromotor with 1200 (grooves / mm) x 500 (blaze, nm) gratings, and a slit selected bandpass of 8 nm. Emission was measured in the right angle geometry with a 5 mm x 5 mm square quartz cuvette through a long-pass filter and dispersed with a 100 x 800 grating onto the array detector. Bandpass for the

emission side was set to 8 nm. Integration time at each excitation wavelength was typically 20s (contour plot). Collected spectra were corrected for the wavelength dependent irradiance of the excitation beam, and the wavelength dependence of the long pass filter and detector train as calibrated to a NIST traceable lamp. For the fluorescence measurements, samples were diluted with 10 g/L DOC in D_2O by a minimum of 1 part sample to 5 parts DOC-D_2O, and a maximum of 1 part sample to 8 parts DOC-D_2O.

SWCNT Species Assignments: Many of the (*n,m*) species contributing to each fraction can be readily assigned by matching multiple peak locations in absorbance data, or from a combination of the peak observed excitation and emission wavelengths in the photoluminescence plots using tabulated data.[7,8] In general, optical features of SWCNTs dispersed in DOC aqueous solutions are red shifted by ≈ (3 – 5) nm for S_{22} transitions and by ≈ (8 – 10) nm for S_{11} transitions with respect to the tabulated values measured in, or extrapolated from, SDS surfactant solution measurements.

REFERENCES

[1] Cheng, H. M.; Li F.; Su; G.; Pan H. Y.; He; L. L.; Sun, X.; Dresselhaus, M. S. Large-Scale and Low-Cost Synthesis of Single-Walled Carbon Nanotubes by the Catalytic Pyrolysis of Hydrocarbons. *Appl. Phys. Lett.***1998**, 72, 3282-3284.

[2] Yu, B.; Liu, C.; Hou, P.; Tian, Y.; Li, S.; Liu, B.; Li, F.; Kauppinen, E. I.; Cheng, H. M. Bulk Synthesis of Large Diameter Semiconducting Single-Walled Carbon Nanotubes by Oxygen-Assisted Floating Catalyst Chemical Vapor Deposition. *J. Am. Chem. Soc.* **2011**, 133, 5232–5235.

[3] Fagan, J. A.; Khripin, C. Y.; Silvera Batista, C.; Simpson, J. R.; Hároz, E. H.; Hight Walker, A. R.; Zheng, M. Isolation of Specific Small-Diameter Single-Wall Carbon Nanotube Species *via* Aqueous Two-Phase Extraction. *Adv. Materials* **2014**, 26, 2800–2804.

[4] Telg, H.; Hároz, E. H.; Duque, J. G.; Tu, X.; Khripin, C. Y.; Fagan, J. A.; Zheng, M.; Kono, J.; Doorn, S.K. Diameter Dependence of TO Phonon Frequencies and the Kohn Anomaly in Armchair Single-Wall Carbon Nanotubes. *Phys. Rev. B* **2014**, 90, 245422.

[5] Cambré, S.; Wenseleers, W. Separation and Diameter-Sorting of Empty (End-Capped) and Water-Filled (Open) Carbon Nanotubes by Density Gradient Ultracentrifugation. *Angew. Chem. Int. Ed.* **2011**, 50, 2764 – 2768.

[6] Fagan, J.A; Huh, J.Y.; Simpson, J.R.; Blackburn, J.L.; Holt, J.M.; Larsen, B.A.; Walker, A.R.H. Separation of Empty and Water-Filled Single-Wall Carbon Nanotubes. *ACS Nano* **2011**, 5, 3943-3953.

[7] Weisman, R. B.; Bachilo, S. M. Dependence of Optical Transition Energies on Structure for Single-Walled Carbon Nanotubes in Aqueous Suspension: An Empirical Kataura Plot. *Nano Lett.* **2003**,3, 1235–1238.

[8] Maultzsch, J.; Telg, H.; Reich,S.; Thomsen, C. Radial Breathing Mode of Single-Walled Carbon Nanotubes: Optical Transition Energies and Chiral-Index Assignment. *Phys. Rev. B* **2005**, 72, 205438.